



Depth-integrated equation for large-scale modelling of low-frequency hydroacoustic waves

P. Sammarco^{1,†}, C. Cecioni², G. Bellotti² and A. Abdolali²

¹Department of Civil and Computer Science Engineering, University of Rome Tor Vergata, Via del Politecnico 1, 00133 Rome, Italy

²Department of Engineering, University of Roma Tre, Via Vito Volterra 62, 00146 Rome, Italy

(Received 5 February 2013; revised 6 March 2013; accepted 8 March 2013)

We present a depth-integrated equation for the mechanics of propagation of low-frequency hydroacoustic waves due to a sudden bottom displacement associated with earthquakes. The model equation can be used for numerical prediction in large-scale domains, overcoming the computational difficulties of three-dimensional models and so creating a solid base for tsunami early warning systems.

Key words: compressible flows, surface gravity waves, topographic effects

1. Introduction

Low-frequency hydroacoustic waves are precursors of tsunamis. Their appeal, i.e. a propagation speed significantly larger than that of the tsunamis, is inversely proportional to the intrinsic difficulty of their measurement, because of their low amplitude and complex wave form evolution. As their appeal is however extremely strong, several analytical investigations have been carried out in order to reveal the physical characteristics of acoustic waves generated by bottom sudden displacement, clarifying that there exists a relationship between the tsunamigenic source and the hydroacoustic waves (Nosov 1999; Chierici, Pignagnoli & Embriaco 2010). Indeed, the idea of using measurements of hydroacoustic waves dates back to the work of Ewing, Tolstoy & Press (1950). The seminal work of Yamamoto (1982) shed light on the physical features of the set of N propagating hydroacoustic modes and the accompanying evanescent ones. By standard application of Fourier and Laplace transforms to the transient problem of inviscid compressible ocean of constant depth subject to a localized displacement, Stiasnie (2010) found an analytical expression

† Email address for correspondence: sammarco@ing.uniroma2.it

for the wave field. In the same work, Stiassnie using the method of stationary phase, also determined the far field, giving explicit formulae for the propagating modes and the induced pressure field. Kadri & Stiassnie (2012) have also analysed the case of a step-like straight discontinuity, an idealized model of the continental shelf effects on waves incoming from deep ocean, and showed that transmitted modes are present for any relative step ratios.

Recent experimental evidence of the existence of low-frequency elastic waves generated by the seabed motion has been found during the Tokachi-Oki 2003 tsunami event. The observatory of the Independent Administrative Institution, Japan Agency for Marine-Earth Science and Technology (JAMSTEC), detected the pressure signal induced by the earthquake (Nosov *et al.* 2007, 2005). Nosov & Kolesov (2007) developed a three-dimensional numerical model, reproducing most of the hydroacoustic wave properties, but predicting a partially wrong peak frequency of the signal. Chierici *et al.* (2010) incorporated into an analytical model the flow in a porous sedimentary bed, greatly improving the agreement of their results with measurements by Nosov & Kolesov (2007).

The complete modelling of these waves could in principle dramatically improve the effectiveness of a tsunami early warning system (TEWS), given the recent advances in deep-sea measurement technology. However, applications to real cases require detailed numerical modelling in order to clearly define the time series at point A due to a source at point B. Three-dimensional models (Nosov & Kolesov 2007) are straightforward to use, but require unrealistic computational times when applied to large-scale geographical areas, i.e. they cannot be used for a systematic investigation on an oceanic scale of prediction. Hence the necessity of a two-dimensional model, based on depth-integrated equations, that can retain all the physical features, yet at the same time be the basis of an efficient prediction tool.

2. The mild-slope equation for hydroacoustic waves

Consider a sample computation carried out using a full three-dimensional solver in a constant-depth domain, where an earthquake is modelled as a unit sudden elevation of the sea bottom. The results are depicted in figure 1, which shows the free-surface elevation η and the corresponding frequency spectrum of the ocean at 50 km from the earthquake. Hydroacoustic waves reach the point ~ 40 s after the initial time of bottom movement. They appear to exist in some narrow frequency bands, with peaks at the cut-off modal frequencies given by Stiassnie (2010). A modelling strategy may take advantage of these filtering effects, by propagating separately each frequency band of the forcing spectrum. In the following we formulate the mathematical problem for a generic single frequency ω of the forcing spectrum. Computations presented later in the paper are carried out for each frequency band and the final results are obtained by simple superposition.

Consider the problem of wave propagation in a weakly compressible inviscid fluid, where waves are generated by a moving bottom and then propagate over a mildly sloped seabed. The seabed vertical distance from the mean water level $z = 0$ is therefore a function of horizontal coordinates x, y and time t , i.e. $z = -h(x, y, t)$.

Depth-integrated modelling of hydroacoustic waves

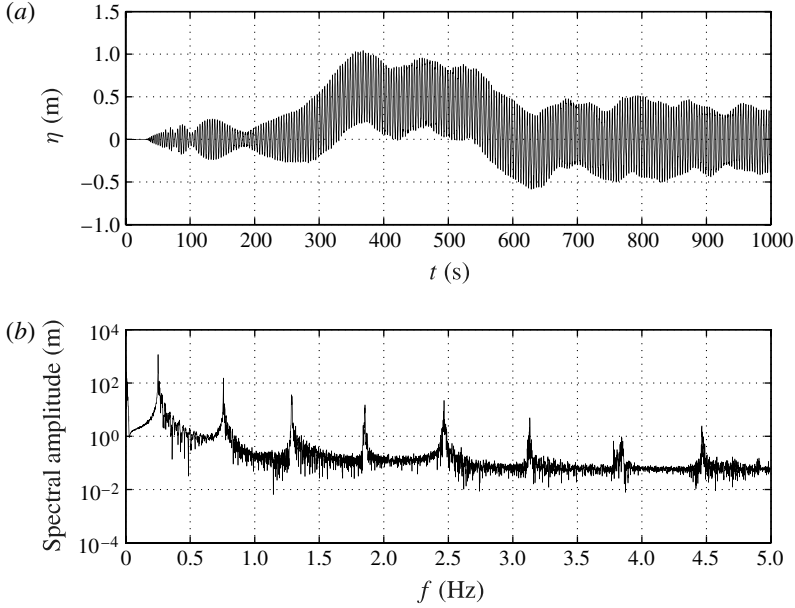


FIGURE 1. Results of a sample computation carried out using a three-dimensional flow solver, showing (a) the free-surface elevation η and (b) the corresponding frequency spectrum of the ocean at $x = 50$ km. The propagation acts as a filter showing energy only at the propagating eigenmodes of the system.

The governing equation and boundary conditions for the fluid potential $\Phi(x, y, z, t)$ are:

$$\left. \begin{aligned} \Phi_{tt} - c_s^2 \nabla^2 \Phi - c_s^2 \Phi_{zz} &= 0, \\ \Phi_{tt} + g \Phi_z &= 0 \quad \text{at } z = 0, \\ \Phi_z + \nabla h \cdot \nabla \Phi + h_t &= 0 \quad \text{at } z = -h(x, y, t), \end{aligned} \right\} \quad (2.1)$$

where ∇ and ∇^2 are respectively the gradient and the Laplacian in the horizontal plane x, y , while subscripts on dependent variables denote partial derivatives and c_s is the (constant) celerity of sound in water. The waves must also be outgoing at infinity. This can be obtained by applying the Sommerfeld radiation condition along a boundary placed at a finite distance from the wave sources (Givoli 1991, 1992).

Similarly to Smith & Sprinks (1975) and Mei, Stiassnie & Yue (2005) we seek the solution of (2.1) by expanding in a series of orthogonal functions, $f_n(z)$, the classic eigenfunctions of the constant-depth homogeneous problem, but with the local $h = h(x, y, t)$:

$$f_n(z) = \frac{\cosh[\beta_n(h+z)]}{\cosh(\beta_n h)}, \quad (2.2)$$

where the β_n are the roots of the dispersion relation

$$\beta_n = \begin{cases} n = 0: & \beta_n = \beta_0, & \omega^2 = g\beta_0 \tanh(\beta_0 h) \\ n \geq 1: & \beta_n = i\tilde{\beta}_n, & \omega^2 = -g\tilde{\beta}_n \tan(\tilde{\beta}_n h). \end{cases} \quad (2.3)$$

The hypothesis of a mild slope allows us to seek a solution in the form:

$$\Phi(x, y, z, t) = \sum_{n=0}^{\infty} \phi_n(x, y, z, t) = \sum_{n=0}^{\infty} \psi_n(x, y, t) f_n(z). \quad (2.4)$$

In order to obtain governing equation and boundary conditions for each of the $\phi_n(x, y, z, t)$ and $\psi_n(x, y, t)$, the forcing term of the bottom boundary condition of (2.1), $h_t(x, y, t)$, must also be expressed in terms of the eigenfunctions $f_n(z)$. Let

$$h(x, y, t) = \sum_{n=0}^{\infty} h_n(x, y, t) f_n(z) \quad \text{for any } z \in [-h, 0] \quad (2.5)$$

and use the orthogonality property of the f_n to obtain the n th expansion coefficient:

$$h_n(x, y, t) = h(x, y, t) \frac{\int_{-h}^0 f_n dz}{\int_{-h}^0 f_n^2 dz} = h(x, y, t) \frac{2 \sinh(2\beta_n h)}{2\beta_n h + \sinh(2\beta_n h)}. \quad (2.6)$$

By virtue of expansions (2.4) and (2.5), the governing equation and boundary conditions (2.1) can be rewritten for each of the ϕ_n as:

$$\left. \begin{aligned} \phi_{n_{tt}} - c_s^2 \nabla^2 \phi_n - c_s^2 \phi_{n_{zz}} &= 0, \\ \phi_{n_{tt}} + g \phi_{n_z} &= 0 \quad \text{at } z = 0, \\ \phi_{n_z} + \nabla h \cdot \nabla \phi_n + h_{n,t} f_n &= 0 \quad \text{at } z = -h(x, y, t), \end{aligned} \right\} \quad (2.7)$$

and equivalently in terms of the ψ_n and f_n as:

$$\left. \begin{aligned} \psi_{n_{tt}} f_n - c_s^2 \nabla^2 \psi_n f_n - c_s^2 \psi_n f_{n_{zz}} &= 0, \\ \psi_{n_{tt}} f_n + g \psi_n f_{n_z} &= 0 \quad \text{at } z = 0, \\ \psi_n f_{n_z} + \nabla h \cdot \nabla \psi_n f_n + h_{n,t} f_n &= 0 \quad \text{at } z = -h(x, y, t). \end{aligned} \right\} \quad (2.8)$$

We still require each of the ϕ_n to be outgoing at infinity. Since

$$\phi_{n_{zz}} = f_{n_{zz}} \psi_n = \beta_n^2 f_n \psi_n = \beta_n^2 \phi_n, \quad (2.9)$$

the first equation of (2.7) can be written as:

$$\frac{1}{c_s^2} \phi_{n_{tt}} - \nabla^2 \phi_n - \phi_{n_{zz}} = \frac{1}{c_s^2} \phi_{n_{tt}} - \nabla^2 \phi_n - \beta_n^2 \phi_n. \quad (2.10)$$

Upon multiplication by f_n and integration over the depth, (2.10) becomes:

$$\int_{-h}^0 \left(\frac{1}{c_s^2} \phi_{n_{tt}} - \nabla^2 \phi_n \right) f_n - \beta_n^2 \phi_n f_n dz = \int_{-h}^0 (\phi_{n_{zz}} f_n - \phi_n f_{n_{zz}}) dz. \quad (2.11)$$

Straightforward application of the Green's identity to the right-hand side of (2.11) yields:

$$\int_{-h}^0 \left(\frac{1}{c_s^2} \phi_{n_{tt}} - \nabla^2 \phi_n - \beta_n^2 \phi_n \right) f_n dz = [f_n \phi_{n_z} - \phi_n f_{n_z}]_0 - [f_n \phi_{n_z} - \phi_n f_{n_z}]_{-h}. \quad (2.12)$$

Depth-integrated modelling of hydroacoustic waves

Since $f_n(z)$ takes the following values at the vertical boundaries:

$$f_n = 1, \quad f_{nz} = \beta_n \tanh(\beta_n h) \quad \text{at } z = 0, \quad (2.13a)$$

$$f_n = 1/\cosh(\beta_n h), \quad f_{nz} = 0 \quad \text{at } z = -h, \quad (2.13b)$$

equation (2.12) becomes:

$$\begin{aligned} & \int_{-h}^0 \left(\frac{1}{c_s^2} \phi_{n_{tt}} - \nabla^2 \phi_n - \beta_n^2 \phi_n \right) f_n \, dz \\ &= -\frac{1}{g} \psi_{n_{tt}} - \psi_n \beta_n \tanh(\beta_n h) + [f_n \nabla h \cdot \nabla \phi_n]_{-h} + \frac{h_{nt}}{\cosh^2(\beta_n h)}. \end{aligned} \quad (2.14)$$

By virtue of the basic properties of the differential operators

$$\nabla \phi_n = \nabla(\psi_n f_n) = f_n \nabla \psi_n + \psi_n \nabla f_n, \quad (2.15a)$$

$$\nabla^2 \phi_n = \nabla^2(\psi_n f_n) = f_n \nabla^2 \psi_n + 2 \nabla \psi_n \cdot \nabla f_n + \psi_n \nabla^2 f_n, \quad (2.15b)$$

equation (2.14) can be rewritten as:

$$\begin{aligned} & \int_{-h}^0 \left(\frac{\psi_{n_{tt}} f_n^2}{c_s^2} - f_n^2 \nabla^2 \psi_n - 2 f_n \nabla \psi_n \cdot \nabla f_n - \psi_n f_n \nabla^2 f_n - \beta_n^2 f_n^2 \psi_n \right) dz \\ &= -\frac{1}{g} \psi_{n_{tt}} - \frac{\omega^2}{g} \psi_n + [f_n^2 \nabla h \cdot \nabla \psi_n]_{-h} + [f_n \psi_n \nabla h \cdot \nabla f_n]_{-h} + \frac{h_{nt}}{\cosh^2(\beta_n h)}, \end{aligned} \quad (2.16)$$

and then, by combining the second and third terms on the left-hand side of (2.16) into $\nabla(f_n^2 \nabla \psi_n)$, (2.16) becomes:

$$\begin{aligned} & \int_{-h}^0 \frac{\psi_{n_{tt}} f_n^2}{c_s^2} \, dz - \int_{-h}^0 \nabla(f_n^2 \nabla \psi_n) \, dz - \int_{-h}^0 \psi_n f_n \nabla^2 f_n \, dz - \int_{-h}^0 \beta_n^2 f_n^2 \psi_n \, dz \\ &= -\frac{1}{g} \psi_{n_{tt}} - \frac{\omega^2}{g} \psi_n + [f_n^2 \nabla h \cdot \nabla \psi_n]_{-h} + [f_n \psi_n \nabla h \cdot \nabla f_n]_{-h} + \frac{h_{nt}}{\cosh^2(\beta_n h)}. \end{aligned} \quad (2.17)$$

By virtue of Leibniz's rule, the second term of the left-hand side can be combined with the third term of the right-hand side, so that (2.17) becomes:

$$\begin{aligned} & \psi_{n_{tt}} \frac{C_n}{c_s^2} - \nabla(C_n \nabla \psi_n) - \beta_n^2 C_n \psi_n + \frac{1}{g} \psi_{n_{tt}} + \frac{\omega^2}{g} \psi_n - \frac{h_{nt}}{\cosh^2(\beta_n h)} \\ &= [f_n \psi_n \nabla h \cdot \nabla f_n]_{-h} + \psi_n \int_{-h}^0 f_n \nabla^2 f_n \, dz, \end{aligned} \quad (2.18)$$

where $C_n(x, y)$ is given by:

$$C_n(x, y) = \int_{-h}^0 f_n^2 \, dz = \frac{2\beta_n h + \sinh(2\beta_n h)}{4\beta_n \cosh^2(\beta_n h)}. \quad (2.19)$$

The two right-hand-side terms of (2.18) are respectively $O(|\nabla h|^2, \nabla^2 h)$. Let k indicate the wavenumber scale of the generic hydroacoustic propagating mode. The case of a mild slope means that $\nabla h \ll kh$, so that the $|\nabla h|^2$ term on the right-hand side is negligible when compared to the left-hand-side terms. Since $\nabla^2 h \ll \nabla h$, in the limit $\nabla h \ll 1$, the second term on the right-hand side can be neglected. Therefore:

$$\psi_{n_{tt}} \frac{C_n}{c_s^2} - \nabla(C_n \nabla \psi_n) - \beta_n^2 C_n \psi_n + \frac{1}{g} \psi_{n_{tt}} + \frac{\omega^2}{g} \psi_n = \frac{h_{nt}}{\cosh^2(\beta_n h)}. \quad (2.20)$$

Recalling expression (2.6) and defining

$$D_n(x, y) = \frac{1}{\cosh^2(\beta_n h)} \frac{\int_{-h}^0 f_n dz}{\int_{-h}^0 f_n^2 dz} = \frac{4 \tanh(\beta_n h)}{(2\beta_n h + \sinh(2\beta_n h))}, \quad (2.21)$$

equation (2.20) assumes its final form:

$$\psi_{n,tt} \left(\frac{C_n}{c_s^2} + \frac{1}{g} \right) - \nabla (C_n \nabla \psi_n) + \left(\frac{\omega^2}{g} - \beta_n^2 C_n \right) \psi_n = h_t D_n, \quad (2.22)$$

which we will name the hyperbolic mild-slope equation for weakly compressible fluids, MSEWC. Note that for an incompressible fluid, i.e. in the limit $c_s \rightarrow \infty$, (2.22) reduces to the classical mild-slope equation (MSE), with β_n the wavenumber and the function $C_n \rightarrow cc_g/g$.

In the form (2.22) the equation still describes all the mechanics in the x, y plane, i.e. the propagating and evanescent modes picture that we would obtain if separation of variables were applied. The MSEWC overcomes the difficulties of finding a fully analytical solution for more complex geometries other than the horizontal or piecewise horizontal in the x, z vertical plane of Stiassnie (2010) and Kadri & Stiassnie (2012). Solution of this equation can be sought once the bottom displacement spectrum is given. The computations can be carried out by dividing the spectrum into frequency bands and by propagating each harmonics separately via (2.22). Note that we do not need prior knowledge of the eigenfrequencies of the propagating modes and how they transform as they propagate (evanescent to propagating or vice versa) as the numerical solution naturally yields the selective filtering effects.

For reference, by taking the Fourier transform of (2.22), the elliptic version of the MSEWC can be found:

$$\nabla (C_n \nabla \Psi_n) + \left(\frac{\omega^2}{c_s^2} + \beta_n^2 \right) C_n \Psi_n = -i\omega H D_n, \quad (2.23)$$

where Ψ_n and H are the Fourier transform of respectively $\psi_n(x, y, t)$ and $h(x, y, t)$.

3. Sample computations

Sample computations have been carried out to verify if the model equation (2.22) can be safely applied instead of more computationally expensive three-dimensional ones. Herein we present the results for two different domains, one with a constant water depth and the other with a varying sea bottom. In the constant-water-depth computation, two models have been used for comparison: a finite-element solver of the full three-dimensional mathematical problem (2.1) and the analytical solution of Stiassnie (2010). The simplified earthquake effect is modelled as a displacement in the vertical direction of the bottom; water depth is 1500 m. The width of the area of the rising bottom is 30 km; and its velocity is 1 m s⁻¹ for a total displacement of 1 m. Frequency bands of width 0.02 Hz have been selected to discretize the forcing spectrum. The numerical solvers are applied on a computational domain 500 km long; given the symmetry of the problem about the mid-point of the earthquake ($x = 0$), computations are undertaken only for half of the physical domain. An appropriate boundary condition is applied at the open end of the domain, so that the waves leave the domain freely. At $x = 0$, a fully reflective boundary condition is used in order to

Depth-integrated modelling of hydroacoustic waves

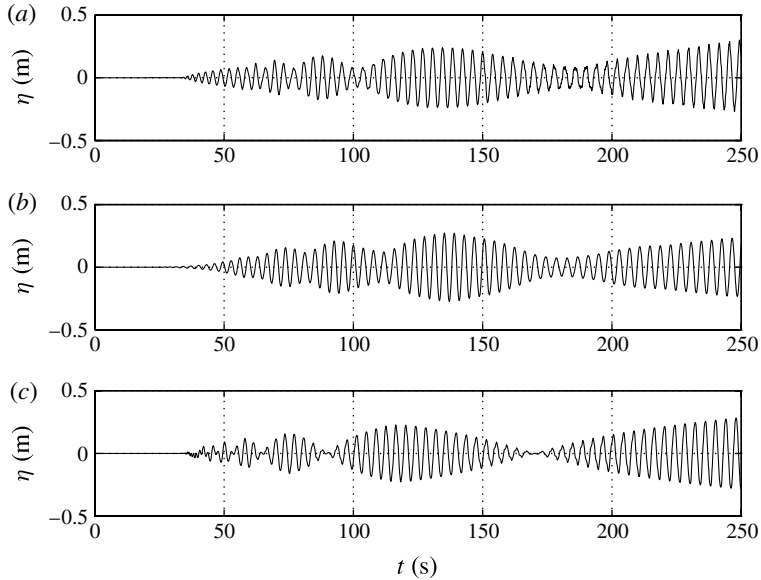


FIGURE 2. Results for the free-surface elevation time series at 50 km from the tsunamigenic source from the three models: (a) three-dimensional model; (b) depth-integrated model; (c) analytical solution.

preserve symmetry. In order to correctly reproduce the wave field, the maximum mesh size is 200 m, for a total of 1250 degrees of freedom (DOF) in the case of the depth-integrated model equation (2.22), and more than 10 000 DOF for the three-dimensional one (2.1). The time step is $t = 0.1$ s and the computational time to reproduce 1000 s of real-time simulation was ~ 1 h for (2.22) and ~ 10 h for (2.1); a computer equipped with an i7 2:67 GHz CPU and 12 GB RAM has been used.

The results are presented in figures 2 and 3 in terms of free-surface elevation η . At $x = 50$ km (figure 2) the two numerical models are in optimal agreement. Both the general structure of the time series and the values of the η are almost identical. The analytical solution by Stiassnie (2010) is still very similar to the two numerical results but some differences exist. At $x = 100$ km (figure 3) there is agreement between the three solutions. However, the depth-integrated model does not show the modulation as well as the other two sample results. Nevertheless the general structure of the time series is still in very good agreement as are the values attained by the η .

In the second case of varying sea bottom, the domain geometry, depicted in figure 4(a), has a 200 km area with a constant water depth of 2 km, an area of 100 km with a sloping bottom, and another area of 200 km with constant water depth of 3.5 km. The model is compared only with the three-dimensional numerical model, as an analytical solution is not readily found. The earthquake is modelled in the shallower area (2 km water depth), it has a width of 45 km and it moves vertically with bottom velocity equal to 2 m s^{-1} for a total displacement of 2 m. The maximum mesh size is again 200 m, for a total of 3000 DOF in the case of the depth-integrated model equation (2.22), and 30 000 DOF for the three-dimensional one (2.1). The time step and the discretization of the spectra are the same as in the constant-depth case. The computational time to reproduce 3000 s of real-time simulation was ~ 2 h

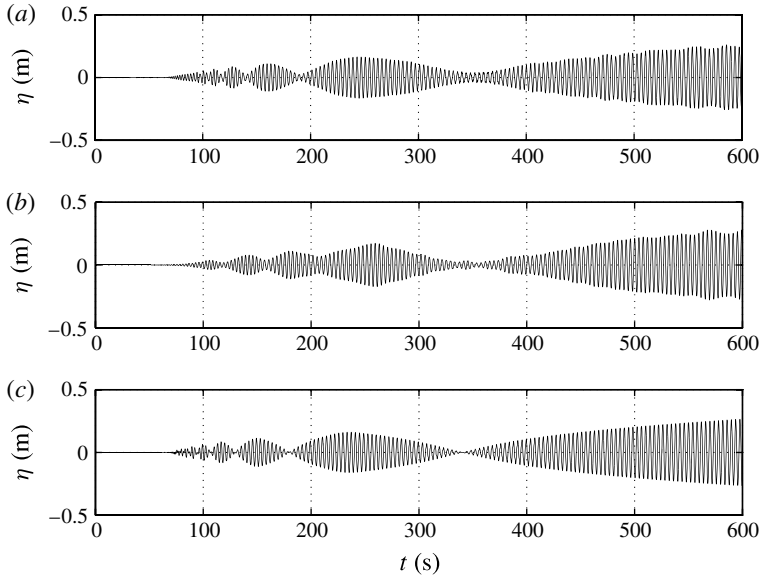


FIGURE 3. Results for the free-surface elevation time series at 100 km from the tsunamigenic source from the three models: (a) three-dimensional model; (b) depth-integrated model; (c) analytical solution.

for (2.22) and ~ 24 h for (2.1), using the same computer as the previous simulation. The results are presented in figure 4(b,c) in terms of free-surface elevation η , at a distance $x = 400$ km from the moving sea bed area. The two time series are in good agreement, both in terms of amplitude and modulation of the signal.

4. Conclusions

The correct detection of hydroacoustic waves generated by sudden displacement of the ocean bottom could enhance significantly the efficiency and promptness of tsunami early warning systems. Hence the need for a full modelling of the phenomenon in the oceans and seas. We have therefore considered a weakly compressible inviscid fluid in which waves are generated by a moving bottom and then propagate over a mildly sloped seabed. Via a proper application of the averaging technique, we have derived a hyperbolic mild-slope equation for weakly compressible fluids (MSEWC). Solution of the equation allows the description of all the mechanics in the x, y plane, overcoming at the same time both analytical and numerical difficulties. On the one hand, by expanding in series of the vertical eigenfunctions, the MSWEC retains semi-analyticity and can be applied to more complex geometries other than the horizontal or piecewise horizontal in the x, z vertical plane as in the seminal work of Stiassnie (2010) and Kadri & Stiassnie (2012). On the other hand, because computational time saving is so dramatic, i.e. one order of magnitude shorter than the fully numerical three-dimensional model, systematic applications supporting a TEWS in the oceans and seas of geophysical interest will be viable. Once a bottom displacement time series and spectrum are given, the computations can be carried out by dividing the spectrum into frequency bands, propagating each harmonic separately and then using superposition. So far the MSWEC has been compared with analytical solutions and three-dimensional

Depth-integrated modelling of hydroacoustic waves

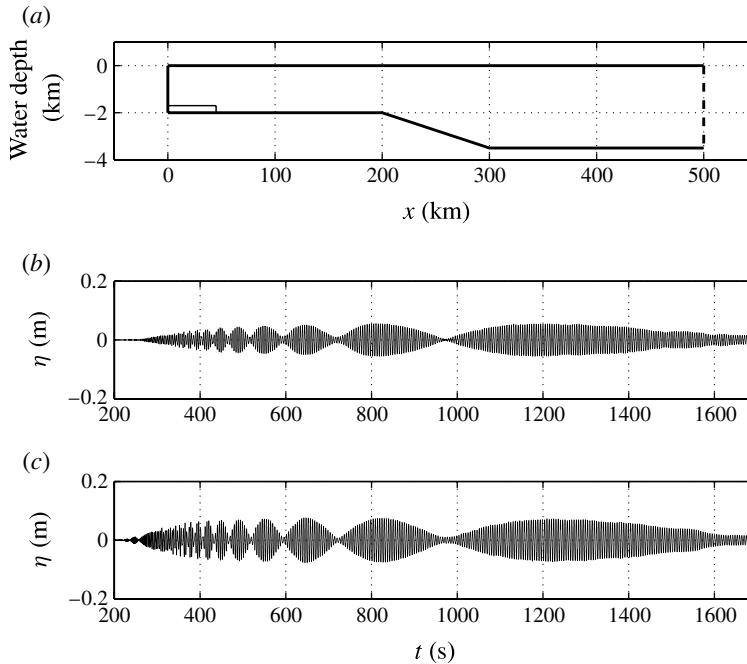


FIGURE 4. The case of varying sea bottom. (a) The computational domain. (b,c) Results for the free-surface elevation time series at 400 km from the tsunamigenic source from the three-dimensional (b) and depth-integrated (c) models.

numerical model results. Work is in progress to obtain reliable field measurements of hydroacoustic waves (Simeone & Viola 2011; Riccobene 2012) related to seismic events, to measure the MSWEC performance against more realistic benchmark data sets.

Acknowledgements

This work was funded by the Italian Ministry of Research (MIUR), under the research project FIRB 2008-FUTURO IN RICERCA (Design, construction and operation of the Submarine Multidisciplinary Observatory experiment). We thank Dr F. Chierici and G. Riccobene for the useful discussions.

References

- CHIERICI, F., PIGNAGNOLI, L. & EMBRIACO, D. 2010 Modeling of the hydroacoustic signal and tsunami wave generated by seafloor motion including a porous seabed. *J. Geophys. Res.* **115**, C03015.
- EWING, M., TOLSTOY, I. & PRESS, F. 1950 Proposed use of the T phase in Tsunami warning systems. *Bull. Seismol. Soc. Am.* **40**, 53–58.
- GIVOLI, D. 1991 Non-reflecting boundary conditions. *J. Comput. Phys.* **94** (1), 1–29.
- GIVOLI, D. 1992 A numerical-solution procedure for exterior wave problems. *Comput. Struct.* **43** (1), 77–84.
- KADRI, U. & STIASSNIE, M. 2012 Acoustic-gravity waves interacting with the shelf break. *J. Geophys. Res.* **117**, C03035.

- MEI, C. C., STIASSNIE, M & YUE, D. K.-P. 2005 *Theory and Applications of Ocean Surface Waves. Part 1: Linear Aspects*, Adv. Series in Ocean Engineering, vol. 23. World Scientific.
- NOSOV, M. A. 1999 Tsunami generation in compressible ocean. *Phys. Chem. Earth B* **24** (5), 437–441.
- NOSOV, M. A. & KOLESOV, S. V. 2007 Elastic oscillations of water column in the 2003 Tokachi-Oki tsunami source: in-situ measurements and 3-D numerical modelling. *Nat. Hazards Earth Syst. Sci.* **7** (2), 243–249.
- NOSOV, M. A., KOLESOV, S. V., DENISOVA, A. V., ALEKSEEV, A. B. & LEVIN, B. V. 2007 On the near-bottom pressure variations in the region of the 2003 Tokachi-Oki tsunami source. *Oceanology* **47** (1), 26–32.
- NOSOV, M. A., KOLESOV, S. V., OSTROUKHOVA, A. V., ALEKSEEV, A. B. & LEVIN, B. V. 2005 Elastic oscillations of water layer in tsunami source. *Dokl. Akad. Nauk* **404** (2), 255–258.
- RICCOBENE, G. 2012 Towards acoustic UHE neutrino detection in the Mediterranean Sea. *Nucl. Instrum. Meth. Phys. Res. A* **692**, 197–200.
- SIMEONE, F. & VIOLA, S. 2011 The SMO project: a submarine multidisciplinary observatory in deep-sea. *Mobile Adhoc and Sensor System International Conference, IEEE-MASS/MARSS*, Valencia (Spain), pp. 898–903, ISBN: 978-1-4577-1345-3.
- SMITH, R. & SPRINKS, T. 1975 Scattering of surface waves by conical island. *J. Fluid Mech.* **72** (2), 373–384.
- STIASSNIE, M. 2010 Tsunamis and acoustic-gravity waves from underwater earthquakes. *J. Engng Maths* **67** (1), 23–32.
- YAMAMOTO, T. 1982 Gravity waves and acoustic waves generated by submarine earthquakes. *Intl J. Soil Dyn. Earthq. Engng* **1** (2), 75–82.